

EVOLUTION OF MICROSTRUCTURE AND EMBRITTLEMENT DURING THE TEMPERING PROCESS IN SiCrCu MEDIUM-CARBON STEELS

RAZVOJ MIKROSTRUKTURE IN KRHKOSTI SREDNJE OGLJIČNEGA JEKLA VRSTE SiCrCu MED NJEGOVIM POSTOPKOM POPUŠČANJA

Pavel Salvetr^{1*}, Aleksandr Gokhman^{1,2}, Črtomir Donik³, Zbyšek Nový¹,
Jabub Kotous¹, Matjaž Godec³

¹COMTES FHT a.s. Prumyslova 995, 334 41 Dobruška, Czech Republic

²South Ukrainian National Pedagogical University (SUNPU), Staroprotfrankivska 26, 65020 Odessa, Ukraine

³Institute of Metals and Technology (IMT), Lepi pot 11, 1000 Ljubljana, Slovenia

Prejem rokopisa – received: 2023-01-13; sprejem za objavo – accepted for publication: 2023-02-10

doi:10.17222/mit.2023.744

The effect of Cu and Si contents on the evolution of embrittlement during a heat treatment consisting of quenching into an oil bath and tempering in the range 200–500 °C was investigated in medium-carbon steels with 0.48 w% and 0.57 w% of C. The results showed that the higher silicon content shifted the tempered martensite embrittlement to higher tempering temperatures. The steels alloyed with Cu had lower notch-toughness values, which worsened with increasing tempering temperature compared to the Cu-free samples. In the investigated tempering temperature range, the following microstructural changes occurred: formation of transition carbides, decomposition of retained austenite, and precipitation of cementite and Cu-particles.

Keywords: medium-carbon steel, tempering martensite embrittlement, microstructure, mechanical properties

V članku je opisana raziskava vpliva vsebnosti bakra in silicija na razvoj krhkosti dveh srednje ogljičnih jekel z 0,48 w% in 0,57 w% ogljika med njuno toplotno obdelavo. Toplotna obdelava ali tako imenovano izboljšanje jekel je bilo sestavljeno iz postopka kaljenja v oljni kopeli s temperature avstenitizacije 900 °C in popuščanja v temperaturnem območju med 200 °C in 500 °C. Rezultati raziskave so pokazali, da višja vsebnost silicija premakne krhkost popuščene martenzita k višjim temperaturam popuščanja. Jekla legirana z bakrom imajo manjšo zarezno žilavost, ki se slabša s poviševanjem temperature popuščanja v primerjavi z jeklom, ki ne vsebuje bakra. V preiskovanem območju temperatur popuščanja so ugotavili, da je prišlo do mikrostrukturnih sprememb, kot so: tvorbe prehodnih karbidov, razpada zaostalega austenita in izločanja cementita ter delcev bakra.

Ključne besede: srednje ogljično jeklo, popuščanje martenzitne krhkosti, mikrostruktura, mehanske lastnosti

1 INTRODUCTION

Low-alloyed, medium-carbon steels achieve superior mechanical properties that reduce a component's weight. They are, therefore, very often used for producing parts for high-strength demands, such as springs for automotive and railway vehicles. Steels are usually alloyed with low contents of other elements like chrome, silicon, manganese, vanadium, niobium, titanium, molybdenum and nickel to improve their mechanical properties.^{1–3} The required mechanical properties – high-strength, reduction in area and toughness – of these materials are achieved by conventional heat treatment consisting of quenching and tempering (QT)^{1,3,4} or quenching and partitioning (QP).^{5–10} The original martensitic microstructure in the hardened state is changed during tempering, and the hexagonal ϵ -(Fe_{2,4}C) and orthorhombic η -transition (Fe₂C) carbides are formed in the microstructure during tempering up to 240 °C. Furthermore,

the retained austenite is decomposed between tempering temperatures of 200–300 °C, and finally, the orthorhombic θ -cementite particles (Fe₃C) are formed^{3,11,12}. Microstructural changes are associated with changes in the mechanical properties. Generally, the decrease in strength and the improvement of plastic properties such as elongation, reduction of area, and impact toughness is expected to occur gradually during tempering. Hardness and ultimate tensile strength decrease with tempering temperature. In contrast, yield strength can increase during tempering at low temperatures up to 300 °C² and a broad spectrum of steels is affected by a sharp decrease in impact toughness during tempering. There are at least two reasons for embrittlement. Firstly, embrittlement usually occurs in low-alloyed steels in the range 250–450 °C, and it is called tempered martensite embrittlement (TME). TME is typically attributed to austenite decomposition into Fe₃C in the interlath region of martensite.^{13–16} The second embrittlement, called temper embrittlement (TE), is caused by the segregation of impurities such as phosphorus, tin, antimony, and arsenic at

*Corresponding author's e-mail:
pavel.salvetr@comtesfht.cz (Pavel Salvetr)

Table 1: Chemical composition of investigated steels (w%).

Steel	Specimen	C	Si	Mn	Cr	Mo	Ni	Cu	Fe
54SiCr6	Steel 1	0.57	1.04	0.71	0.77	0.063	0.105	1.54	Bal.
	Steel 2	0.58	2.01	0.70	0.78	0.059	0.120	1.55	
42SiCr	Steel 3	0.42	1.84	0.65	1.40	0.047	0.106	1.41	
	Steel 4	0.43	1.88	0.65	1.40	0.048	0.112	0.04	

prior austenite grain boundaries in Cr-Mo and Ni-Cr-Mo steels. The dangerous temperature interval for TE is stated to be between 450 °C and 650 °C.^{14,17,18} The irreversible TME should exhibit transgranular fracture through the prior austenite grains, whereas the reversible TE leads to intergranular failure along the existing prior austenite grain boundaries.¹⁶ Nevertheless, the features of TME and TE may be very similar, and it could be challenging to separate them. The stated temperature ranges for TE and TME are not entirely consistent and vary depending on the chemical composition of the steel. Generally, the reason for the embrittlement occurrence in tempered steels can be attributed to the heat treatment accompanied by several phase transformations such as decomposition of retained austenite, interlath precipitation or coarsening of cementite particles and impurities segregation.^{16,19} Using steel with as few impurities as possible and avoiding dangerous tempering temperatures is a way to limit failure due to embrittlement formed during tempering.

The current work describes the susceptibility to embrittlement of two medium-C SiCr spring steels during tempering up to 500 °C. This phenomenon can cause a sudden failure of structural parts. Therefore, thorough mechanical testing of new modifications in the chemical composition of steels has to be carried out. The effect of silicon and copper contents on embrittlement during tempering was evaluated using the measurement of impact toughness and observation of the fracture surface.

2 EXPERIMENTAL PART

The chemical compositions of the vacuum-induction-melted 54SiCr6 and 42SiCr steels studied in this work are shown in **Table 1**. An optical emission spectrometer Bruker Q4 TASMAN was used to determine the chemical composition of the steels. To investigate the effects of Si, the Si contents were varied in the range 1–2 w% of silicon in the 54SiCr6 steel. In addition, the effect of Cu was studied and compared to Cu-free (0.04 w%) and 1.41 w% Cu contents in the 42SiCr steel. The ingots were heated up to 1050 °C, hot-rolled to a thickness of 14 mm and air-cooled. Following this a full annealing was carried out at 850 °C for 40 min. Cylindrical samples 120 mm in length and 13 mm in diameter were manufactured and heat treated. Both 54SiCr6 and 42SiCr steel samples were austenitized at 900 °C for 20 min, followed by oil quenching. Subsequently, tempering was carried out in the t range 200–500 °C for 120 min for both steels.

Charpy V-notch impact testing at room temperature was performed on three samples for each treatment route using a Charpy pendulum WPM PSd 300 J (Kögel Werkstoff- und Materialprüfsysteme GmbH, Wachau, Germany) in accordance with SN EN ISO 148-1. Charpy pendulum WPM PSd 300 J (Kögel Werkstoff- und Materialprüfsysteme GmbH, Wachau, Germany) and ČSN EN ISO 148-1. Charpy V notch specimens were prepared with (55 × 10 × 5) mm dimensions and a 2-mm V notch depth. After the tests, the fracture surfaces were observed using a scanning electron microscope (SEM).

Specimens were prepared for microstructural investigation in the scanning electron microscope (SEM) JEOL IT 500 HR (JEOL, Tokyo, Japan) by grinding and polishing. The microstructure was revealed by etching in 2 % Nital solution (98 ml H₂O + 2 ml HNO₃).

X-ray diffraction (XRD) analysis was performed on the polished surfaces of samples on a Bruker Advance D8 diffractometer with a copper anode ($\lambda K_{\alpha 1} = 0.15406$ nm). The content of retained austenite (RA) was determined in the 2θ range from 35° to 85° with a step size of 0.025°.

EBS (Electron backscatter diffraction) maps were acquired with a EDAX Hikari camera (EDAX, Mahwah, NJ, USA) on the polished surface of the 54SiCr6 steel samples (tempered at 200 °C and 500 °C) under the following conditions: 20 kV, on an area of (40 × 40) μm and step size of 0.05 μm , 5 × 5 binning, scanning speed 55 points per second, tilted for 70°. The data acquisition and post-processing were performed using the software TEAM 4.5 (EDAX LLC, Mahwah, NJ, USA) and EDAX OIM Analysis™ Version 8.0 (EDAX LLC, Mahwah, NJ, USA). EBSD maps were cleaned by the “grain dilation” procedure with a grain tolerance angle and minimum grain size of 5 points. The value of the confidence index was set to higher than 0.15. EBSD analyses provided results of grain size, misorientation angle and dislocation density.

3 RESULTS AND DISCUSSION

3.1 Impact toughness and fracture surface observation

The Charpy impact test brought basic knowledge about the embrittlement of steels during tempering, see **Table 2**.

The impact toughness of the 54SiCr steel specimens reached values of about 16–17 J/cm² after quenching and tempering (QT) at 200 °C in contrast to 14 J/cm² for Steel 1 and Steel 2 after quenching. The impact tough-

ness decreased with elevated tempering temperature to 300 °C. The tempering temperature of 300 °C represents the local minimum in impact toughness for Steel 1. A further increase in tempering temperature led to an enhancement of impact toughness values of Steel 1, whereas the loss of impact toughness continued in Steel 2 at the tempering temperature of 400 °C. After tempering at 500 °C, values of the impact toughness of Steel 1 and Steel 2 did not change significantly.

Table 2: Evolution of notch impact toughness during tempering between 200 °C and 500 °C.

Sample/KCV (J/cm ²)	Tempering temperature			
	200 °C	300 °C	400 °C	500 °C
Steel 1	16.4	12.6	18.1	18.3
Steel 2	17.3	15.3	9.7	9.6
Steel 3	29.1	29.4	17.9	10.4
Steel 4	25.4	23.9	23.0	18.6

In the case of 42SiCr steel specimens, the impact toughness of Steel 4 decreased slightly up to the tempering temperature of 400 °C after QT, in contrast to 12 J/cm² for Steel 4 and 14 J/cm² for Steel 3 after quenching. The decrease in impact toughness was accelerated in the Cu-alloyed sample (Steel 3) at tempering temperatures of 400 °C and 500 °C. Based on the summary of impact toughness values in **Table 2**, the effect of copper and silicon on the impact toughness and TME

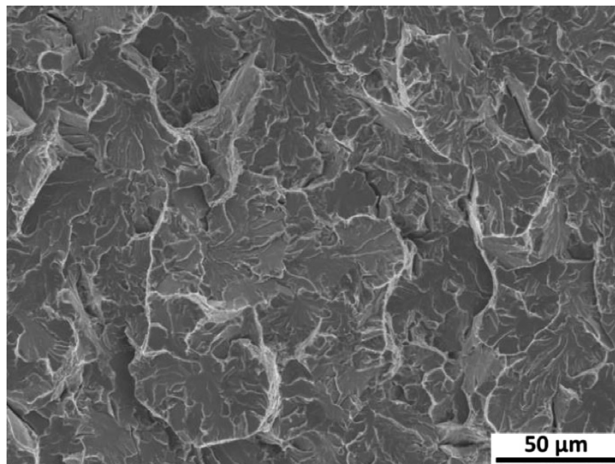


Figure 1: Fracture surface of Steel 2 in the as-quenched state

can be assessed. Firstly, alloying with copper deteriorates the impact toughness and promotes TME. The big difference in impact toughness between steel with and without Cu occurs mainly at higher tempering temperatures of 400 °C and 500 °C. The effect of Si consists of shifting the TME range to higher tempering temperatures, as seen by comparing the impact toughness values of specimens Steel 1 and Steel 2.

Fracture surfaces of the impact-toughness-tested specimens at 20 °C were examined in **Figure 1** and **Figure 2**. For a demonstration of the fracture surface evolu-

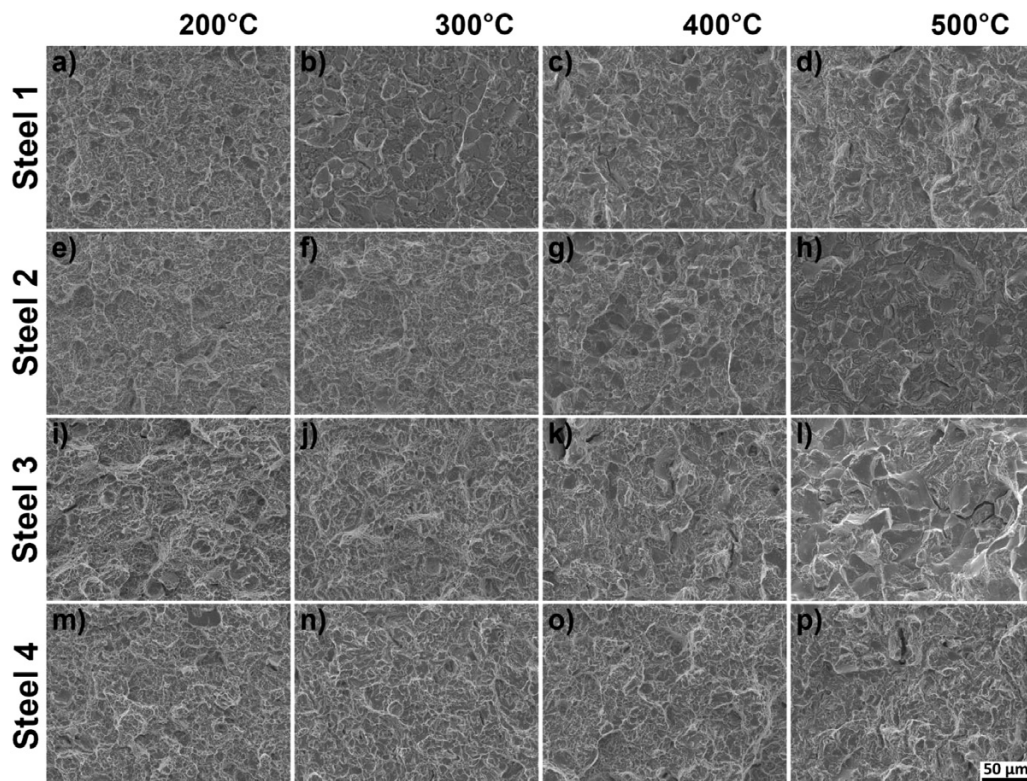


Figure 2: Fracture surfaces of Steel 1 tempered at 200 °C – a), 300 °C – b), 400 °C – c), 500 °C – d); Steel 2 tempered at 200 °C – e), 300 °C – f), 400 °C – g), 500 °C – h); Steel 3 tempered at 200 °C – i), 300 °C – j), 400 °C – k), 500 °C – l) and Steel 4 tempered at 200 °C – m), 300 °C – n), 400 °C – o) and 500 °C – p).

tion, the fracture examination of the as-quenched state on **Figure 1** was added, and it revealed typical signatures for brittle transgranular fracture typical for as-quenched martensite. After tempering at 200 °C, the fracture characteristics of samples Steel 1 and Steel 2 changed to ductile fracture with dimples on the fracture surface. After tempering at 300 °C, a mixed mode of intergranular fracture with a faceted appearance and transgranular fracture with a dimple morphology was observed in Steel 1. In contrast, the fracture surface of Steel 2 remained similar to the previous one. The tempering at 400 °C caused a similar appearance of fracture surfaces of both samples (Steel 1 and Steel 2), and the mixed modes of fracture were observed. The intergranular fracture left smooth facets revealing grain boundaries, while transgranular regions were covered with dimples. The characteristics of the mixed fracture mechanism also remained after tempering at 500 °C on the fracture surfaces of both Steel 1 and Steel 2. The intergranular fracture took a larger fraction of the fracture surface in Steel 2 compared to Steel 1.

In the case of 42SiCr steel samples Steel 3 and Steel 4, fracture surfaces with transgranular features and dimples were observed after tempering at 200 °C and 300 °C for Steel 3 and additionally at 400 °C for Steel 4. At the fracture surface of Steel 3 tempered at 400 °C, facets and cleavage began to appear, indicating a weakening of the grain boundaries. The change to a mixed fracture mode in Steel 3 was revealed by increasing the tempering temperature to 500 °C. The typical signs of brittle–intergranular fracture, such as facets and triple points, dominate at the fracture surface. In contrast, the fracture mechanism of Steel 4 tempered at 500 °C was still predominantly transgranular.

3.2 Microstructure analysis

The microstructure development of medium-carbon steels, represented by sample Steel 1, is shown in **Figure 3** after tempering ranging from 200 °C to 500 °C. All samples tempered up to 400 °C exhibit a similar microstructure, which is composed of martensite, ϵ - and η -transition carbides and retained austenite (**Figure 3a**). In addition, ferritic grains were observed in 42SiCr steel samples (**Figure 4**). The quenching temperature was too low, although the same quenching temperature was used for the 42SiCr in previous works.^{20–22} The area fraction of ferrite reached 2.9 ± 0.9 % for both 42SiCr steels. Martensite is created by packets, blocks and lath, typical for these steels described in the previous studies.^{23–25} At the tempering temperature of 400 °C and above, the precipitation of cementite particles appears (**Figure 3b**). Cementite precipitates along PAGB and lath boundaries and within martensite lath as well being visible in SEM microstructure after tempering at 500 °C, as shown **Figure 3c**. Nevertheless, it is necessary to mention that the precipitation of Cu particles occurs at tempering at 500

°C, and the influence of Cu precipitates must also be included in the evaluation of notch toughness in the conclusions.²⁶

The influence of chemical composition and mainly carbon and silicon contents on the decomposition of retained austenite is summarized in **Table 3**. There is a substantial difference in the RA amount after tempering

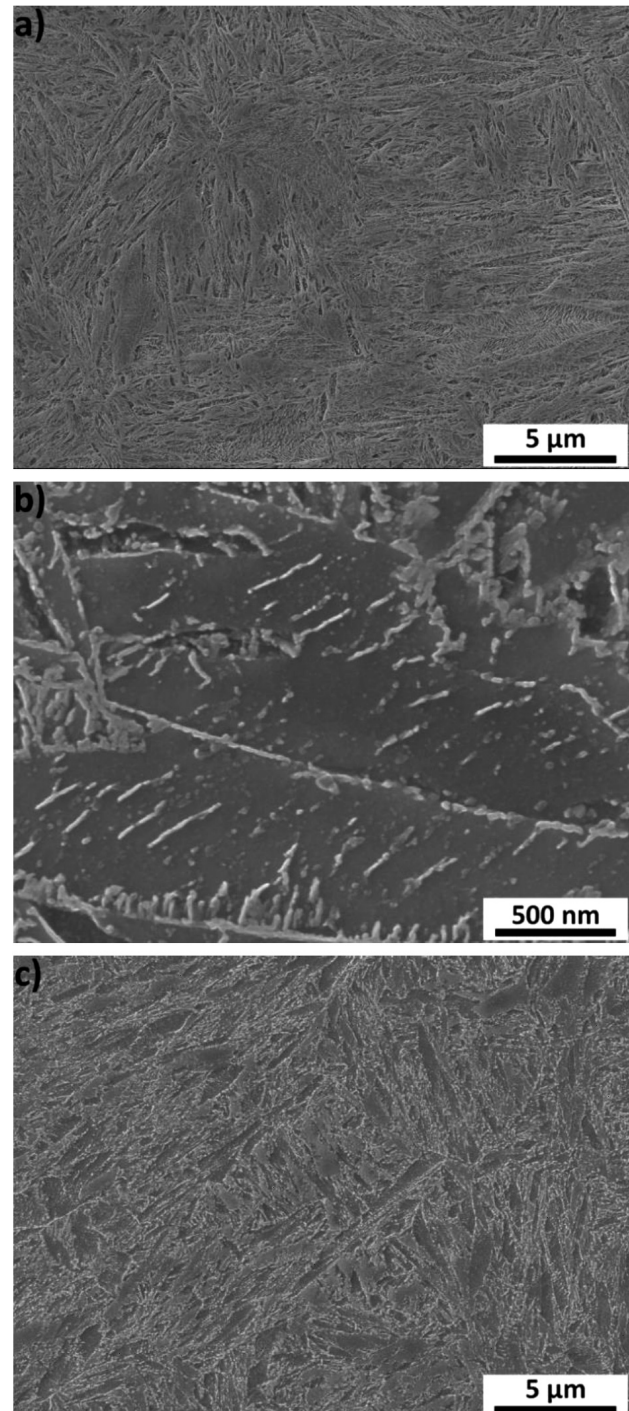


Figure 3: Development of microstructure of Steel 1 during tempering: a) 200 °C, b) 400 °C (detail of precipitated cementite at PAGB), and c) 500 °C

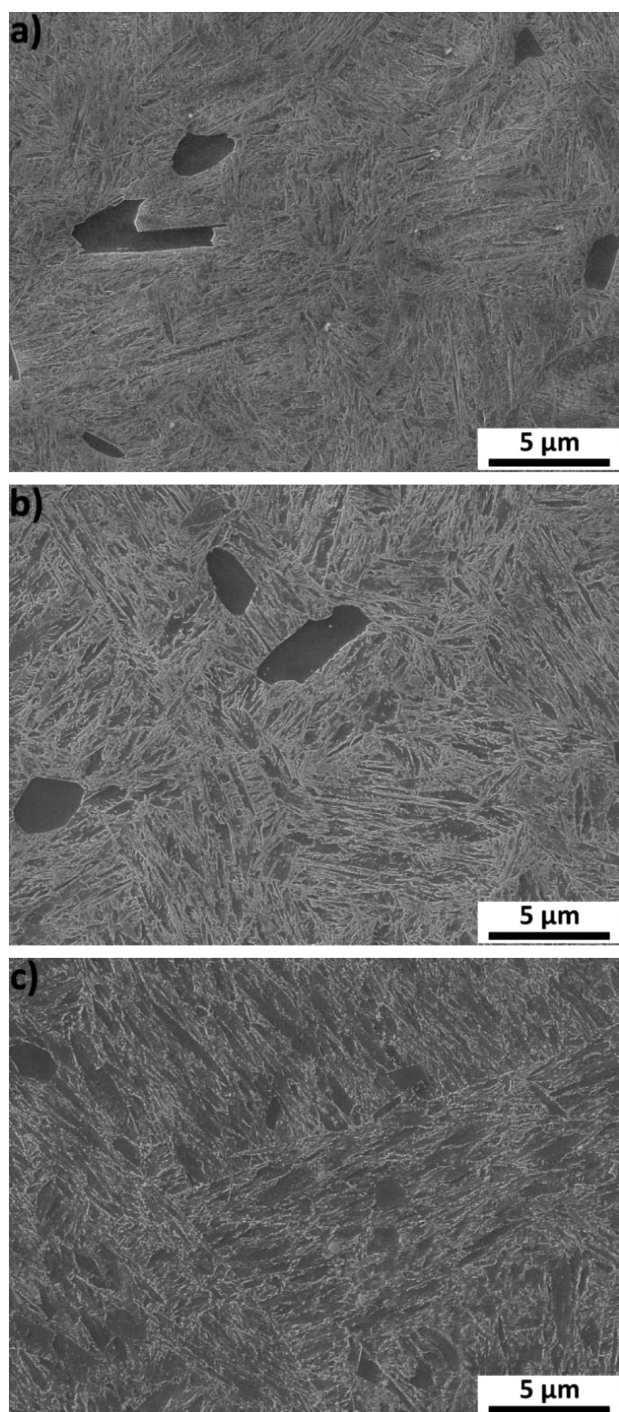


Figure 4: Development of microstructure of Steel 4 during tempering: a) 200 °C, b) 400 °C, and c) 500 °C

at 400 °C because the RA amounts were below 2 w/% or completely decomposed in the samples of Steel 1 at this tempering temperature, while the RA content between 7.0 φ 1% and 9.5 φ 1% was determined in the high-silicon samples (Steel 2, Steel 3 and Steel 4) as is listed in **Table 3**. XRD patterns of the samples tempered at 400 °C are shown in **Figure 5**. It seems that silicon delays the RA decomposition. Very similar RA contents were found in the steel with 0.55 w/% of C and 1.98 w/% of Si in a

previous study and the drop in RA content occurred at the tempering temperature of 450 °C³. The same RA amount evolution was determined for Steel 3 and Steel 4 – the RA content was lower due to the lower C content. Still, the RA decomposition started above the tempering temperature of 400 ° due to a high silicon content. The Cu content does not influence the RA amount in the microstructure significantly.

Table 3: RA content in medium carbon steel during tempering.

Sample/RA (φ 1%)	Tempering temperature			
	200 °C	300 °C	400 °C	500 °C
Steel 1	11.5	10.5	< 2.0	–
Steel 2	12.0	12.5	9.5	–
Steel 3	10.5	8.5	7.0	–
Steel 4	9.5	8.0	7.5	–

Changes in microstructures of the 54SiCr6 steel samples (Steel 1 and Steel 2) during tempering depending on the Si content were evaluated using EBSD analysis. The IPF maps reveal various martensite lath orientations within one PAG (**Figure 6** and **Figure 7**). The low-angle boundaries (5°–15°) are indicated by the red line, and the high-angle boundaries (15°–65°) are demonstrated by the black line in **Figure 6** and **Figure 7**. Geometrically necessary dislocation (GND) maps offer dislocation density distribution maps, and the GND parameter provides an estimation of the dislocation density in the microstructures.²⁷ The higher strain and dislocation density are concentrated near the martensite lath boundaries, as demonstrated by the green colour (**Figure 6** and **Figure 7**). The increase in tempering temperature from 200 °C to 500 °C caused a significant decrease in the

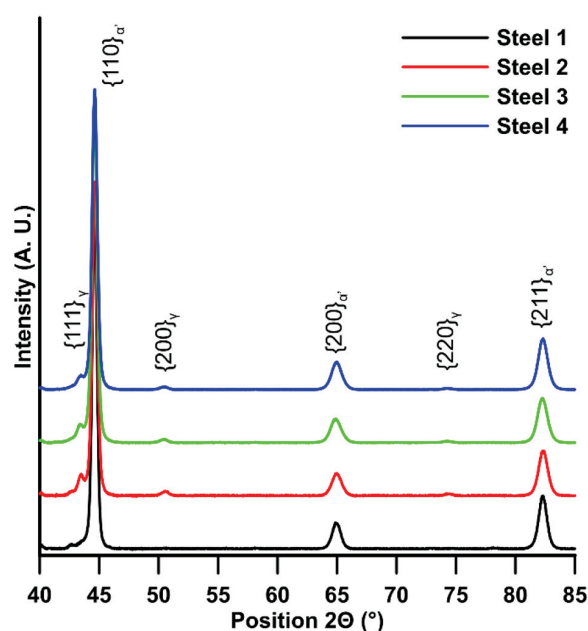


Figure 5: XRD patterns of investigated steels collected after tempering at 400 °C

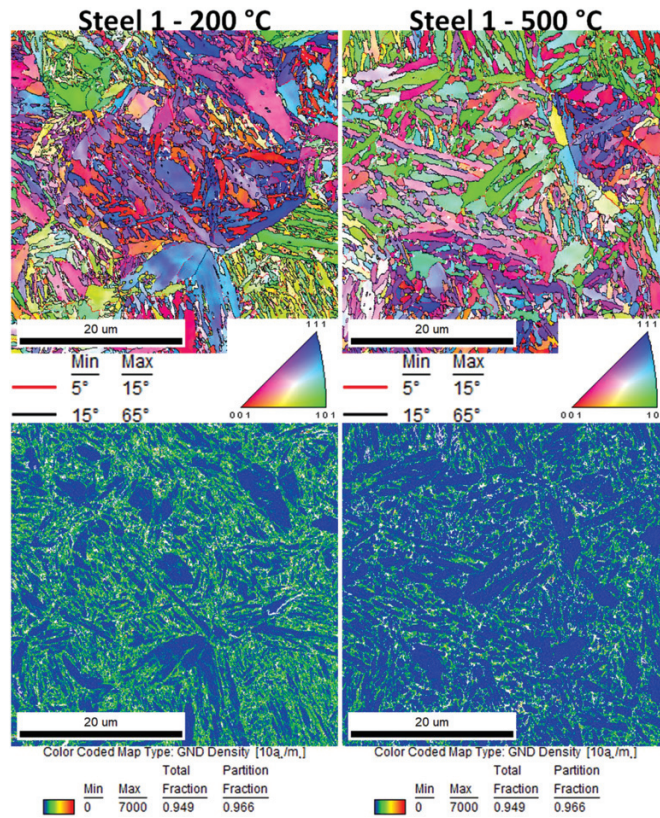


Figure 6: Inverse pole figure in the Z direction (IPF-Z) and geometrically necessary dislocations density maps (GND) for Steel 1 tempered at 200 °C and 500 °C

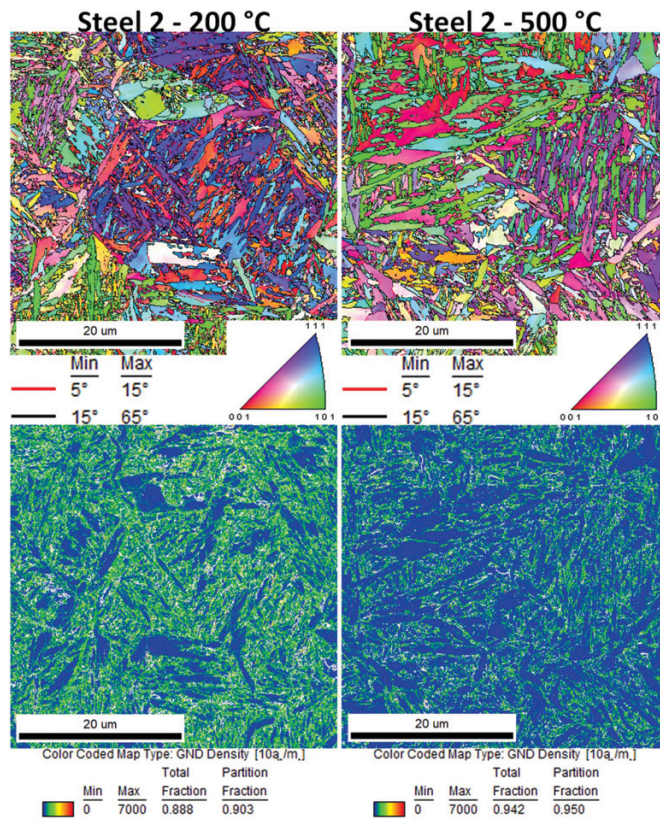


Figure 7: Inverse pole figure in the Z direction (IPF-Z) and geometrically necessary dislocations density maps (GND) for Steel 2 tempered at 200 °C and 500 °C

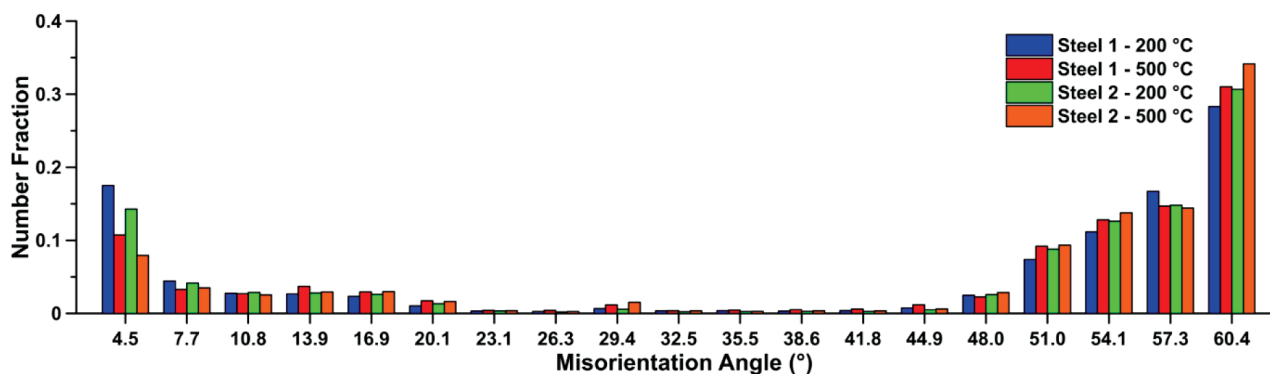


Figure 8: Misorientation angle distribution of samples Steel 1 and Steel 2 tempered at 200 °C and 500 °C

dislocation density in all the investigated samples. The GND values are listed in **Table 4**.

All the samples' equivalent diameter of grains, denoted as grain size (GS), ranges from 0.37 μm to 0.62 μm (**Table 4**). The values of GS correspond well to the results of other studies dealing with similar steels, which reported GS values from 0.4 μm to 0.6 μm .^{28,29} Furthermore, these GS values were evaluated for HAGBs ($> 15^\circ$), similarly as in previous work²⁹ because HAGBs are considered a barrier for dislocation movement. Nevertheless, several works reported that also LAGBs can contribute to strengthening.^{24,30,31}

Table 4: Dislocation density and grain size determined by EBSD analysis.

Sample	Tempering temperature	GND	GS
		(m^{-2})	(μm)
Steel 1	200 °C	$9.08 \cdot 10^{14}$	0.49
	500 °C	$6.42 \cdot 10^{14}$	0.62
Steel 2	200 °C	$1.02 \cdot 10^{15}$	0.37
	500 °C	$7.05 \cdot 10^{14}$	0.44

Figure 8 compares the samples according to the silicon content and the tempering temperature from the misorientation angle distribution. The majority of boundaries belong to misorientations between 3° – 20° and above 45° , while microstructure rarely contains boundaries with misorientations angles from 15° to 45° . The fraction of angles with misorientations between 54° – 60° corresponds to some orientation relationships between austenite and martensite, such as Nishiyama-Wassermann and Kurdjumov-Sachs.^{25,32} As reported in previous works, a similar misorientation angle distribution is usual in quenched and tempered medium-carbon steels.^{1,28,29,33–35} No dependence of misorientation angle on the silicon content was followed. Only a slightly higher fraction of LAGB with a misorientation below 10° was evaluated in samples tempered at 200 °C, compared to samples tempered at 500 °C.

4 CONCLUSIONS

Medium-carbon-steel samples with tempered martensite microstructure were investigated. The relationship between the notch impact toughness and the microstructure (amount of retained austenite, effective grain size, grain boundaries misorientation angle distribution) was evaluated depending on the copper and silicon contents.

- Increasing silicon content delays tempering and shifts the temperature range of the tempered martensite embrittlement to higher tempering temperatures.
- Formation of the carbide film along the grain boundaries causes a sharp decrease in impact toughness.
- The presence of ferrite in the microstructure improves the impact toughness.
- Copper (segregation and clusters) alloying decreases the impact toughness. The impact toughness drops at high tempering temperatures in materials with a high content of silicon and copper, simultaneously.
- The misorientation-angle distribution with a high fraction of grain boundaries below 15° and between 54° – 60° was found using EBSD, as is usual for quenched and tempered medium-carbon steels.

Acknowledgment

The paper was supported within the project Research of advanced steels with unique properties, No. CZ.02.1.01/0.0/0.0/16_019/0000836, financed from ERDF.

5 REFERENCES

- 1 K. Chen, Z. Jiang, F. Liu, J. Yu, Y. Li, W. Gong, Ch. Chen, Effect of quenching and tempering temperature on microstructure and tensile properties of microalloyed ultra-high strength suspension spring steel, *Mater Sci Eng A.*, 766 (2019), 138272, doi:10.1016/j.msea.2019.138272
- 2 W.-J. Nam, H.-C. Choi, Effects of silicon, nickel, and vanadium on impact toughness in spring steels, *Mater Sci Technol.*, 13 (1997) 7, 568–574, doi:10.1179/mst.1997.13.7.568
- 3 S. Teramoto, M. Imura, Y. Masuda, T. Ishida, M. Ohnuma, Y. Neishi, T. Suzuki, Influence of Iron Carbide on Mechanical Properties in

- High Silicon-added Medium-carbon Martensitic Steels, *ISIJ Int.*, 60 (2020) 1, 182–189, doi:10.2355/isijinternational.ISIJINT-2019-331
- ⁴ P. Salvetr, A. Gokhman, Z. Nový, P. Motyčka, J. Kotous, Effect of 1.5 wt% Copper Addition and Various Contents of Silicon on Mechanical Properties of 1.7102 Medium Carbon Steel, *Materials*, 14 (2021) 18, 5244, doi:10.3390/ma14185244
- ⁵ T. Janda, H. Jirková, Š. Jeníček, L. Kučerová, Influence of Cooling Rate on Microstructure and Mechanical Properties of 42SiCr Steel after Q&P Process, *Manuf Technol.*, 19 (2019) 4, 583–588, doi:10.21062/ujep/338.2019/a/1213-2489/MT/19/4/583
- ⁶ Š. Jeníček, K. Opatová, J. Hajšman, I. Vorel, Evolution of Mechanical Properties and Microstructure in Q&P Processed Unconventional Medium-Carbon Silicon Steel and Comparison between Q&P Processing, Quenching and Tempering, and Austempering, *Manuf Technol.*, 22 (2022) 2, 146–155, doi:10.21062/mft.2022.026
- ⁷ Z. Xiong, P.-J. Jacques, A. Perlade, T. Pardoen, Ductile and intergranular brittle fracture in a two-step quenching and partitioning steel, *Scr Mater.*, 157 (2018), 6–9, doi:10.1016/j.scriptamat.2018.07.030
- ⁸ M. Liu, J. Guan, Q. Zhang, L. Ai, L. Fan, G. Xu, Microstructure and Properties of a Medium-Carbon Ti-Mo-Bearing Steel Treated by One-Step Quenching and Partitioning Treatment, *J Mater Eng Perform.*, 31 (2022) 1, 297–304, doi:10.1007/s11665-021-06198-x
- ⁹ J. Lu, H. Yu, P. Kang, X. Duan, C. Song, Study of microstructure, mechanical properties and impact-abrasive wear behavior of medium-carbon steel treated by quenching and partitioning (Q&P) process, *Wear*, 414–415 (2018), 21–30, doi:10.1016/j.wear.2018.07.026
- ¹⁰ D. Sun, S. Huang, C. Chen, H. Wang, X. An, Q. Li, X. Huang, Enhancement of the Mechanical Properties of a V–Ti–N Microalloyed Steel Treated by a Novel Precipitation-Quenching & Partitioning Process, *Metall Mater Trans A Phys Metall Mater Sci.*, 53 (2022) 10, 3696–3712, doi:10.1007/s11661-022-06778-z
- ¹¹ G.R. Speich, W.C. Leslie, Tempering of steel. *Metall Trans.*, 3 (1972) 5, 1043–1054, doi:10.1007/BF02642436
- ¹² S. Primig, H. Leitner, Separation of overlapping retained austenite decomposition and cementite precipitation reactions during tempering of martensitic steel by means of thermal analysis, *Thermochim Acta.*, 526 (2011) 1–2, 111–117, doi:10.1016/j.tca.2011.09.001
- ¹³ S. S. M. Tavares, R. P. C. da Cunha, C. Barbosa, J. L. M. Andia, Temper embrittlement of 9%Ni low carbon steel, *Eng Fail Anal.*, 96 (2019), 538–542, doi:10.1016/j.engfailanal.2018.11.011
- ¹⁴ J. P. Materkowski, G. Krauss, Tempered martensite embrittlement in SAE 4340 steel, *Metall Trans A.*, 10 (1979) 11, 1643–1651, doi:10.1007/BF02811697
- ¹⁵ H. Kwon, C.H. Kim, Tempered martensite embrittlement in Fe-Mo-C and Fe-W-C steel. *Metall Trans A.*, 14 (1983) 7, 1389–1394, doi:10.1007/BF02664822
- ¹⁶ F. Zia-Ebrahimi, G. Krauss, Mechanisms of tempered martensite embrittlement in medium-carbon steels, *Acta Metall.*, 32 (1984) 10, 1767–1778, doi:10.1016/0001-6160(84)90233-5
- ¹⁷ J. Pietikainen, Observations about tempered martensite embrittlement, *Scand J Metall.*, 34 (2005) 1, 1–6, doi:10.1111/j.1600-0692.2005.00701.x
- ¹⁸ J. H. Bulloch, D. Crowe, Embrittlement observed in Cr-Mo turbine bolts after service, *Theor Appl Fract Mech.*, 29 (1998) 1, 59–66, doi:10.1016/S0167-8442(98)00016-0
- ¹⁹ M. Sarikaya, A.K. Jhingan, G. Thomas, Retained austenite and tempered martensite embrittlement in medium carbon steels, *Metall Trans A.*, 14 (1983) 6, 1121–1133, doi:10.1007/BF02670450
- ²⁰ I. Vorel, Š. Jeníček, J. Káňa, K. Ibrahim, V. Kotěšovec, B. Mašek, Effect of silicon content on microstructure of low-alloy Q&P-Processed steels, *IOP Conf Ser Mater Sci Eng.*, 179 (2017), 012068, doi:10.1088/1757-899X/179/1/012068
- ²¹ H. Jirková, L. Kučerová, B. Mašek, The Effect of Chromium on Microstructure Development During Q-P Process, *Mater Today Proc.*, 2 (2015), S627–S630, doi:10.1016/j.matpr.2015.07.362
- ²² I. Černý, D. Mikulová, J. Šís, B. Mašek, H. Jirková, J. Malina, Fatigue properties of a low alloy 42SiCr steel heat treated by quenching and partitioning process, *Procedia Eng.*, 10 (2011), 3310–3315, doi:10.1016/j.proeng.2011.04.546
- ²³ E. I. Galindo-Nava, P. E. J. Rivera-Díaz-del-Castillo, A model for the microstructure behaviour and strength evolution in lath martensite, *Acta Mater.*, 98 (2015), 81–93, doi:10.1016/j.actamat.2015.07.018
- ²⁴ C. Sun, P. Fu, H. Liu, H. Liu, N. Du, Y. Cao, The Effect of Lath Martensite Microstructures on the Strength of Medium-Carbon Low-Alloy Steel, *Crystals*, 10 (2020) 3, 232, doi:10.3390/cryst10030232
- ²⁵ S. Morito, H. Tanaka, R. Konishi, T. Furuhashi, T. Maki, The morphology and crystallography of lath martensite in Fe-C alloys, *Acta Mater.*, 51 (2003) 6, 1789–1799, doi:10.1016/S1359-6454(02)00577-3
- ²⁶ A. Gokhman, Z. Nový, P. Salvetr, V. Ryukhtin, P. Strunz, P. Motyčka, J. Zmeko, J. Kotous, Effects of Silicon, Chromium, and Copper on Kinetic Parameters of Precipitation during Tempering of Medium Carbon Steels, *Materials*, 14 (2021) 6, 1445, doi:10.3390/ma14061445
- ²⁷ L. Kubin, A. Mortensen, Geometrically necessary dislocations and strain-gradient plasticity: a few critical issues, *Scr Mater.*, 48 (2003) 2, 119–125, doi:10.1016/S1359-6462(02)00335-4
- ²⁸ F. Liu, K. Chen, C. Kang, Z. Jiang, S. Ding, Effects of V–Nb microalloying on the microstructure and properties of spring steel under different quenching-tempering times, *J Mater Res Technol.*, 19 (2022) 1, 779–793, doi:10.1016/j.jmrt.2022.05.043
- ²⁹ B. Kim, E. Boucard, T. Sourmail, D. San Martín, N. Gey, P.E.J. Rivera-Díaz-del-Castillo, The influence of silicon in tempered martensite: Understanding the microstructure–properties relationship in 0.5–0.6wt.% C steels, *Acta Mater.*, 68 (2014), 169–178, doi:10.1016/j.actamat.2014.01.039
- ³⁰ H. Ghassemi-Armaki, R. P. Chen, K. Maruyama, M. Yoshizawa, M. Igarashi, Static recovery of tempered lath martensite microstructures during long-term aging in 9–12% Cr heat resistant steels, *Mater Lett.*, 63 (2009) 28, 2423–2425, doi:10.1016/j.matlet.2009.08.024
- ³¹ C. Du, J. P. M. Hoefnagels, R. Vaes, M. G. D. Geers, Block and sub-block boundary strengthening in lath martensite, *Scr Mater.*, 116 (2016), 117–121, doi:10.1016/j.scriptamat.2016.01.043
- ³² B. Hutchinson, J. Hagström, O. Karlsson, D. Lindell, M. Tornberg, F. Lindberg, M. Thuvander, Microstructures and hardness of as-quenched martensites (0.1–0.5%C), *Acta Mater.*, 59 (2011) 14, 5845–5858, doi:10.1016/j.actamat.2011.05.061
- ³³ M. S. Suh, S.H. Nahm, C. M. Suh, N. K. Park, Impact Toughness of Spring Steel after Bainite and Martensite Transformation, *Metals*, 12 (2022) 2, 304, doi:10.3390/met12020304
- ³⁴ D. Liu, M. Luo, B. Cheng, R. Cao, J. Chen, Microstructural Evolution and Ductile-to-Brittle Transition in a Low-Carbon MnCrMoNiCu Heavy Plate Steel, *Metall Mater Trans A Phys Metall Mater Sci.*, 49 (2018) 10, 4918–4936, doi:10.1007/s11661-018-4823-9
- ³⁵ K. Zhang, M. Zhu, B. Lan, P. Liu, W. Li, Y. Rong, The Mechanism of High-Strength Quenching-Partitioning-Tempering Martensitic Steel at Elevated Temperatures, *Crystals*, 9 (2019) 2, 94 doi:10.3390/cryst9020094